J Nanotechnol Nanomaterials. 2023;4(1)19-28.

Journal of Nanotechnology and Nanomaterials Research Article

Natural and Forced Convection in Multi-Phasic Electrochemical Systems

S. Abdelghani-Idrissi[1], M.BA. Freville[2], A. Colin[2,*]

[1]Laboratoire de Physique de l'Ecole Normale Supérieure, ENS, Université PSL, CNRS, Sorbonne Université, Université de Paris, Paris, France

[2]MIE - Chemistry, Biology and Innovation (CBI) UMR8231, ESPCI Paris, CNRS, PSL Research University, 10 Rue Vauquelin, Paris, France

[*]Correspondence should be addressed to Annie Colin, annie.colin@espci.fr

Received date: April 14, 2023, **Accepted date:** June 06, 2023

Citation: Abdelghani-Idrissi S, Freville MBA, Colin A. Natural and Forced Convection in Multi-Phasic Electrochemical Systems. J Nanotechnol Nanomaterials. 2023;4(1):19-28.

Abstract

Multi-phasic electrochemical systems such as electrolyzers or metal-air batteries are intimately linked to energy transition and are at the heart of new scientific advances and modern industrial development. The presence of gas phases, inherent to the processes, directly impacts the performance and stability of the systems. In this study, we propose different ways to improve the dynamics of bubble evacuation, through forced convection (flow systems), and natural convection (electrode design and cell geometry). By analyzing the links between the electrochemical kinetics and active surface electrode variations, we show that forced convection is an excellent way to decrease the overall energy cost and reduce the harmful impact of gas bubbles. Regarding natural evacuation, adapted electrode or cell designs also allow to improve performances, without adding external hydraulic circuit.

Keywords: Electrochemistry, Sustainable development, Multi-phasic environments

Introduction

The context of sustainable development calls for the development of new technologies closely related to the water-energy nexus. In order to meet the growing need of energy, metal-air batteries (storage systems) and electrolyzers (H_2 production) are becoming crucial elements for the energy transition.

These electrochemical technologies are based on mechanisms involving a gas phase generation inside a liquid electrolyte. These systems are then characterized by the presence of 3 phases (solid electrode, liquid electrolyte, and generated gas phase) [1]. The control of the evacuation of the gaseous phases is an important point which directly impacts the energy performances and the stability of the systems [2]. In the last ten years different technologies have been proposed to limit the impact of gas bubbles on the electrodes. Chu et al. [3], inspired by the breathing mechanism, proposes to work with porous electrodes which allow the arrival and departure of gas without the formation of bubbles. Other studies reported that structuration of the electrode surfaces at the micron scale may facilitate the gas bubble release and avoid the pinning of large bubbles at the electrode surface [4-5]. Despite improving the bubble departure from electrode surface, new materials for efficient electrocatalyst of hydrogen production (HER) have been recently proposed by Chang Ming et al. [6,7].

From a more fundamental point of view, the study of the impact of bubbles on these systems brings new information on the oscillatory behaviors in electrochemical processes [8-13]. The analysis of the impact of gaseous phases on the systems allows to improve both the fundamental understanding of the interactions between electrodes, electrolyte and reaction products, but also the performances of existing technologies.

With this in mind, we propose in this paper to summarize

different possibilities to improve the diphasic fluidic involved in these systems. Effect of forced and natural convection are studied and quantified in different situations. We focus here on: flow systems and cell geometries. These experimental results are coupled with numerical simulations to find and understand the keys for the optimization of such devices. Strategies for the synthesis of new electrode materials are proposed.

Materials and Methods

The two systems studied in the present work corresponds to a Pt-C electrolyzer and a Zn-O_2 battery submitted to charge conditions.

Electrolyte:

For the Platinum-Carbon cell, the electrolyte used to study the effect of the flow on the electrode potentials is an 8M aqueous solution of potassium hydroxide. This electrolyte is prepared by dissolving KOH (Sigma-Aldrich) in deionized water. The high concentration of hydroxide ions ensures the high conductivity of the solution.

For the Zn-air cell, electrolyte containing zincate ions is used to ensure zinc electrodeposition. Supersaturated 8M KOH 1 M $Zn(OH)_4^{2-}$ electrolyte is obtained by a first dissolution under agitation regime of 12M (336gr) of KOH (ACS reagent, ≥ 85%, pellets, from Sigma-Aldrich), in 500 mL of distilled water. These 12 M of KOH are required since 4 moles of hydroxide react with 1 mole of zinc (see equation below). Solid zinc (zinc sheet, 99.7% purity, GoodFellow) is then electrochemically oxidized to zincates inside the solution by following the half-reaction:

$$Zn + 4OH^- \rightarrow Zn(OH)_4^{2-} + 2e^-$$

In order to avoid zinc deposition at the counter electrode, 2 compartments separated by a cationic membrane (Nafion HP) are used. The two compartments initially contain a 12 M KOH solution. By applying current, zinc dissolution occurs at the anode, while HER is performed on a Nickel counter electrode (inside the other compartment). This way, the dissolute zinc cannot be deposited at the counter electrode because of the selective properties of Nafion HP membranes, and in the other hand, crossover of hydroxide anions is prevented.

Millifuidics cells, electrodes and hydraulic circuit

Since the 2 studied processes are a Pt-C electrolyzer and a Zn-O_2 battery in charging mode, both Pt-C and Zn-Ni electrochemical flow cells are designed.

The electrochemical cells were 3D-printed by stereolithography (SLA) using a Formlabs 3D-printer (Form 3, Formlabs). The studied designs are represented in **Figure 1a**. The electrodes are placed inside the central zone (see central arrows in **Figure 1a**), which area is 3.75 cm^2 (1.5 x 2.5 cm). As shown in **Figure 1a**, several flow-geometries are studied: a 3 channels flow and a V-shape geometry inspired from microfluidic designs. In the Zn-Ni electrochemical flow cell situation, we use two V-shaped geometries with two different distances (gaps) between the two electrodes (1 mm and 2 mm).

All electrode materials were obtained from GoodFellow (platinum plate, zinc plate, Ni grid), the Nickel grid electrode has a mesh size of 550 microns. Electrode potential measurements are made using an Ag/AgCl reference electrode (3 M KCl, saturated with silver chloride from Sigma-Aldrich), in order to isolate the potential of both working and counter electrode.

A peristaltic pump (VWR PP3300) was used to impose the flowing conditions. Electrolyte reservoir is connected to the cell using tubing from Saint-Gobin (PharMed BPT) compatible with these highly basic solutions (internal radius: 3 mm).

Electrochemical experiments: A Bio-Logic potentiostat (VSP, Biologic) was used to perform electrochemical measurements.

In the Pt-C electrolyzer, oxidation of water occurs at the platinum electrode whereas reduction occurs at the carbon electrode:

Pt electrode: $4\,OH^- \rightleftarrows 2\,H_2O_{liq} + O_{2\,gaz} + 4e^-$ (OER)

C electrode: $2\,H_2O_{liq} + 2e^- \rightleftarrows H_2 + 2\,OH^-$ (HER)

Inside the Zn cell, OER occurs at the Ni electrode while Zn deposition occurs at the zinc electrode, the electrochemical reactions that occur during the charging phase are described below:

Ni electrode: $4\,OH^- \rightarrow O_2 + 2\,H_2O + 4\,e^-$ (OER)

Zn electrode: $Zn(OH)_4^{2-} + 2e^- \rightarrow Zn + 4OH^-$ (Zn electro-deposition)

For all experiments, flowing conditions are imposed before the electrical loads. Between each experiment, flowing conditions are imposed during 10 minutes in order to flush the residual bubbles and concentration gradients inside the cell.

The chronopotentiometry experiment protocol is the following: firstly, the system is flushed by applying a 3 mL. s^{-1} flow for 10 minutes. Then the electrolyte flow is fixed to its desired value (0 mL. s^{-1} for static experiments, and 1.5 mL. s^{-1} for flowing experiments) and the current is applied for 10 minutes. The studied current densities are: 3, 10, 20, and 50 mA. cm^{-2}. The potential of the electrodes is recorded by the potentiostat at a sampling frequency of 1 Hz. This protocol is inspired from previous studies regarding gas evolving electrodes [2].

Cyclic voltammetry (CV) experiments are performed by applying a potential ramp at a fixed scan rate of 20 mV. s^{-1}. Tafel parameters are deduced from typical CV experiments [2]. We find $i_0 = 1.89\ 10^{-5}$ A and $\frac{\alpha zF}{RT} = 20$ for the platinum electrode and $i_0 = 7\ 10^{-3}$ A and $\frac{\alpha zF}{RT} = 13.9$ for the Nickel grid.

Analysis of the chronopotentiometry experiments

Our goal is to measure the surface masked by the bubbles during the electrochemical reaction and to determine the overpotential associated with this phenomenon. For this we analyze the electrochemical reactions. Our analysis is based on electrochemical kinetic descriptions, according to Butler-Volmer equation and previous theoretical models [1,7].

The expression of the voltage at a gas evolving electrode measured versus a reference electrode can be expressed as:

$$E(t) - E^{eq} = \frac{RT}{\alpha zF}\left(ln\left(\frac{I(t)}{I_0}\right) + ln\left(\frac{S_0}{S(t)}\right)\right) = \frac{RT}{\alpha zF}\, ln(I(t)) + \eta(t)$$

(Equation 1).

Where $\eta(t)$ is the overpotential and encompasses two terms. The first one $\eta_i = -\frac{RT}{\alpha zF} ln(i_0)$ is linked to the kinetics of the reaction at the electrodes, the second one $\eta_b = \frac{RT}{\alpha zF} ln\left(\frac{S_0}{S(t)}\right)$ corresponds to the variation of the active surface and takes into account the masking of the electrodes by the produced gas bubbles. α and i_0 are extrapolated from Tafel experiments [14] (**Figure 1b**).

One can deduce from this relation the evolution of the free surface which depends on measured potential:

$$\frac{S(t)}{S_0} = \frac{i}{i_0}\, exp\left(-\frac{\alpha zF}{RT}(E(t) - E^{eq})\right)$$ (Equation 2).

These equations can be used to estimate the evolution of the free surface from potential measurements at fixed imposed current. The parameters α and i_0 are obtained from the Tafel plots in **Figure 1b**. The theoretical relationship between overvoltage and free surface is thus plotted in **Figure 1c**. This inverse logarithmic function underlines several important points: when the surface of the electrode is strongly covered, the overvoltage reaches high values. Moreover, the variations

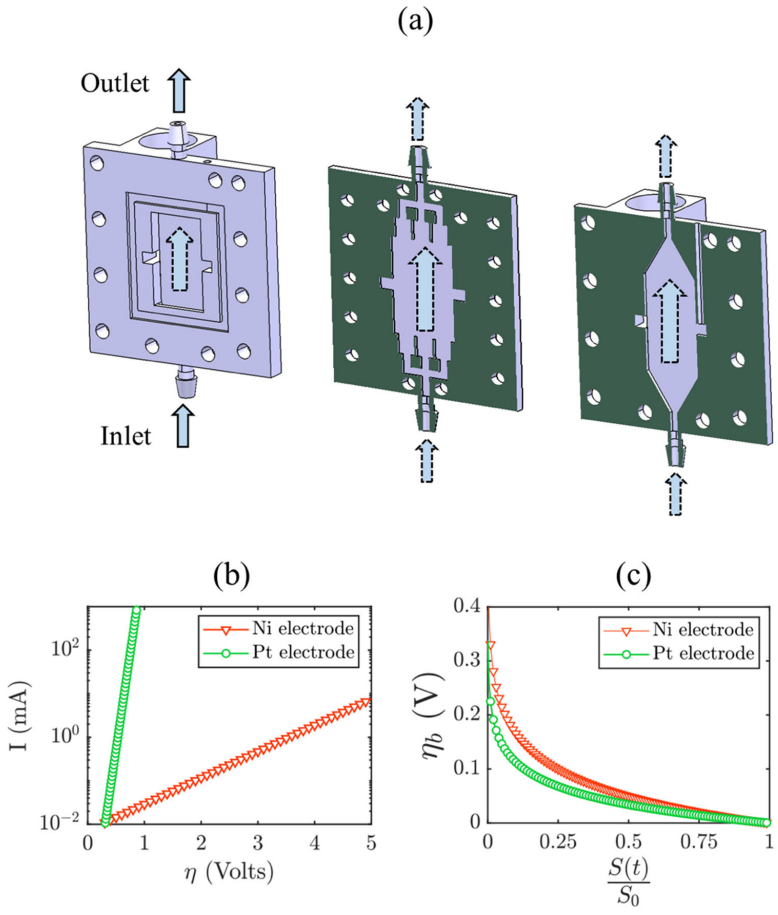

Figure 1: CAD of the electrochemical flow cells and cross-sections for the 2 flow designs studied here **(a)**. Linear Tafel functions for the 2 electrodes studied here **(b)**. Relation between overpotential and free surface **(c)**.

-even small- in this zone of strong covering led to very important variations of potential. Indeed, we notice that:

$(\partial\eta(t)/\partial S(t)) = -(1/S(t))$ (Equation 3).

Which implies high variations and sensitivity to small bubble detachment at low free surfaces.

This theoretical angle is used all along this study in order to link electrochemical kinetics to free surface variations. Since platinum shows the best OER catalytic performances and is well-known to be a model electrode for bubble generation, we will mainly focus on this electrode in the first part of this study. Comparative measurement on both electrodes in optimal configuration will be presented at the end of this section.

Results

Comparison of the V shaped and Channel geometries

We use chronopotentimetry experiments and the previous analysis to compare the different modes of bubble evacuation. For this purpose, we focus on the Pt-C electrolyzer and more precisely on the evolution of the OER reaction at the Platinum electrode. The electrolyte is an 8M aqueous solution of potassium hydroxide. We start by studying the behavior of the cell under forced convection.

Forced convection

Figures 2a-2f represent the deduced surface overpotential and free surface dynamics for several imposed current at a fixed flow rate of 1.5 mL. s^{-1}. Previous results reported that electrolyte flow decreases the overvoltage of these types of devices [1,8]. Results in **Figure 2** confirm this statement and show that adapted flow design inspired by microfluidic systems can drastically improve this effect. When imposed current increases, the 3-channel geometry is not enough performant to allow fast bubble evacuation. It results an important increase of overpotential due to a free surface decrease as reported in **Figure 2**.

However, triangular geometry allows to maintain a low overpotential: as represented in **Figure 2c & 2d**. The free surface using this geometry is higher, meaning that gas accumulation is avoided.

Natural convection

Despite the cell design influence on flowing performances, we can get interested on the natural convection in absence of any external forces. Improving the performances in these conditions allows to avoid the addition of external hydraulic circuit. Results of chronopotentiometry without flowing

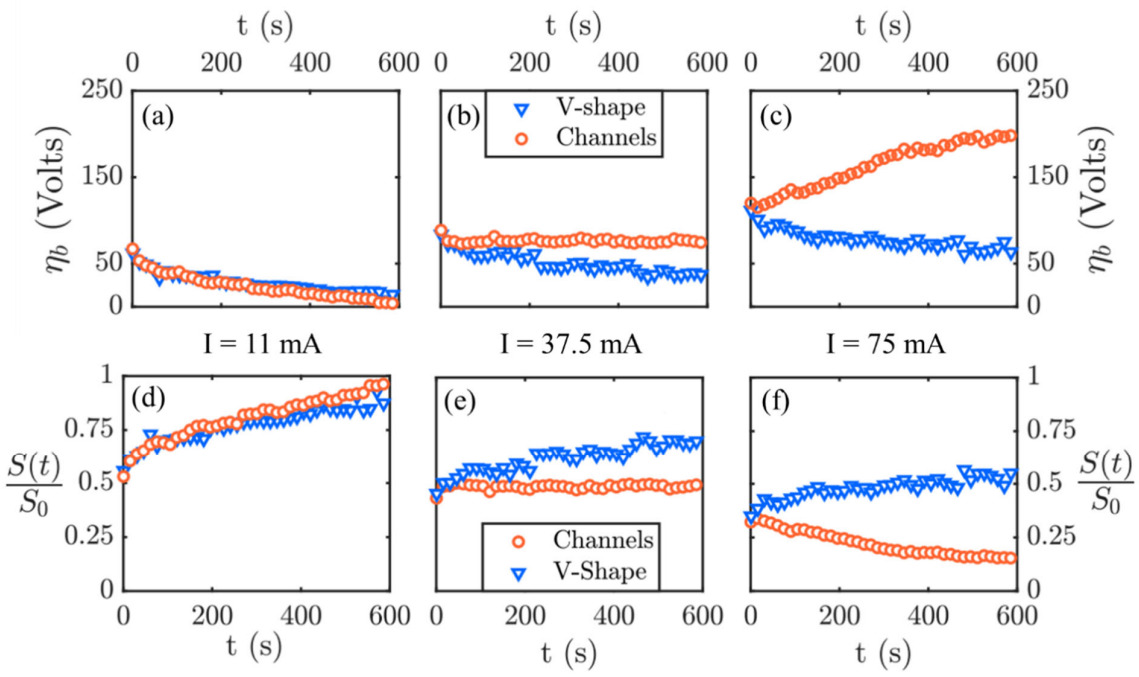

Figure 2: Results of chronopotentiometry experiments under electrolyte flow (Q = 1.5 mL. s^{-1}) for i = 11 mA, 37.5 mA and 75 mA (from left to right). Chart **(a)** to **(c)** represent the overpotential due to surface coverage, while **(d)** to **(f)** represent the deduced free surface.

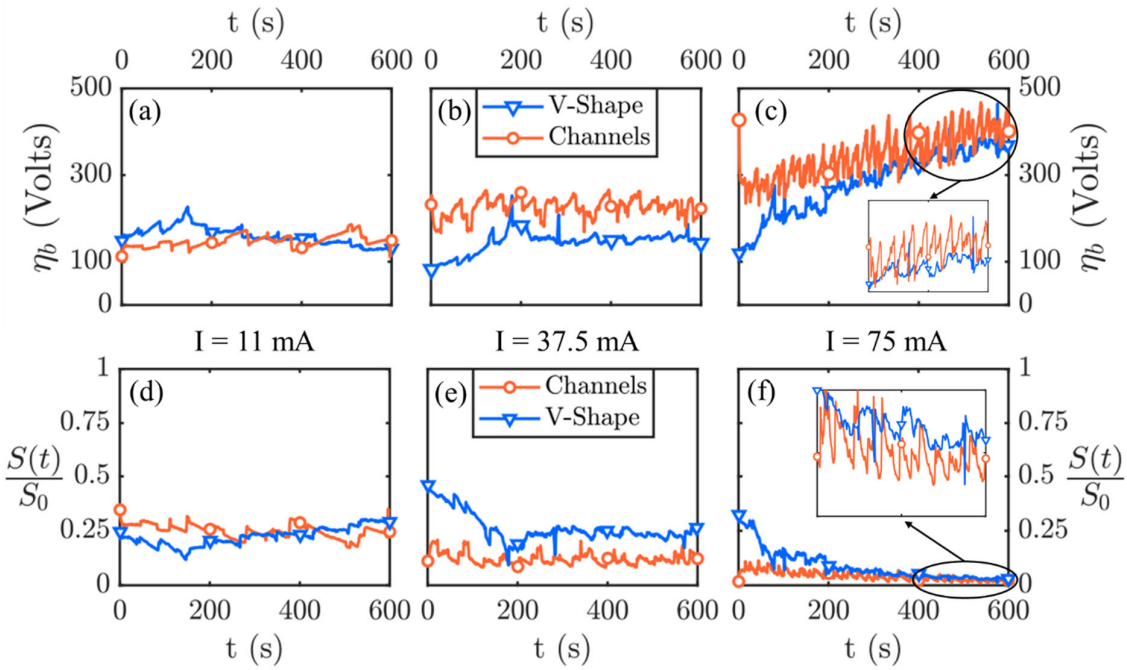

Figure 3: Results of chronopotentiometry experiments under natural convection for i = 11 mA, 37.5 mA and 75 mA (from left to right). Chart **(a)** to **(c)** represent the overpotential due to surface coverage, while **(d)** to **(f)** represent the deduced free surface.

electrolyte are shown in **Figure 3**. As expected, overpotentials and free surface are respectively much higher and lower than the experiments under flowing conditions. Oscillations induced by bubble detachment increase with imposed current, these fluctuations can make the measured signals highly unstable as reported in **Figure 3c & 3f**. Comparison between these natural convection results to the ones presented in **Figure 2** highlights that flowing electrolyte reduces the detachment radius (Fritz radius) and suppresses electrode instabilities. When imposed current increases, measured free surface fluctuates towards 0 which leads to high variations of electric signals and performances as recalled by **Equation 2** and **Figure 1c.** Comparing geometries shows that natural convection occurs in a favorable way for the V-shaped geometry. At moderate and high current, the overpotential is slightly lower for V-shaped geometry.

Moreover, at high imposed current the triangular flowing design allows to partially limit the instabilities observed in channel design, as shown in **Figure 3c**. This difference should signify differences in natural convection occurring at fast gas generation. Indeed, the deduced free surfaces plotted in **Figure 3f** show that channel geometry presents high frequency peaks towards 0, meaning unstable and brutal detachments when the system is mostly covered by bubbles. However, V-shaped geometry shows a slightly smoother signal, and a decrease of the frequency of the detachment peaks.

Fast charge with optimal convection

The results shown in **Figures 2 & 3** underline the benefits of V-shaped geometry, under flowing electrolyte and natural convection. Because of the importance of fast charges for electrochemical technologies, we will now focus on this V-shaped flow-cell under larger current. Both Zinc-Air battery and electrolyzer are studied with respectively Ni and Pt OER electrodes.

Results of electrode potential measurement at 187 mA (50 mA. cm^{-2}) are presented in **Figure 4**. For both electrodes, the overpotential reaches high values without flowing electrolyte. Forced convection allows to reduce the overpotential from 3.5 to 1 V, which corresponds to an energy gain of 70% in this extreme condition. Despite the flow effects, **Figure 4a** shows that the natural convection occurring in this geometry still prevents instabilities for Pt electrode. On Ni OER electrode (**Figure 4b**), the system is stable before 5 min, until it reaches an oscillating and unstable regime. This difference with observed behavior in **Figure 4a** may be attributed to the specific geometry of Ni grid and confirms the role of electrode design showed in **Figure 4b**.

This analysis confirms the advantages of V-shaped geometry for natural convection, and strongly underlines the importance of well-designed flow systems for the fast charge of gas-evolving electrochemical technologies.

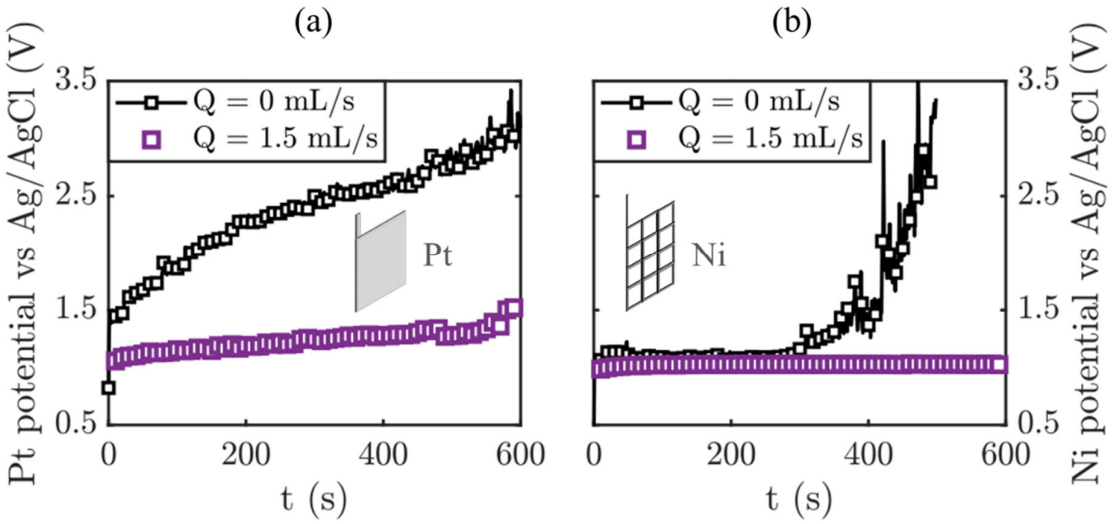

Figure 4: Fast charge chronopotentiometry experiments (I = 50 *mA. cm*$^{-2}$). **(a)** Platinum electrode. **(b)** Ni electrode.

Fast charge: Influence of the gap in the V shaped geometry

Beyond the shape of the channels, the distance between the electrodes, in the presence or absence of forced flow is an important parameter. It is interesting to reduce this distance to decrease the resistance of the cell or to densify the energy per unit volume. However, reducing this distance can be counterproductive as we will see in the following. To study this point, we will focus our study on the Zinc Air battery. During the charging process, oxygen is produced at the nickel electrode. We analyze the charge of the system at 20 mA. cm^{-2}.

Figure 5b shows the influence of the gap for the Zinc Air battery under different flowing conditions. The flow rate being the same in both experiments means that the velocity is 2 times smaller in the 2 mm gap than in the 1 mm gap. The shear stress that causes the bubbles to detach from the surface is

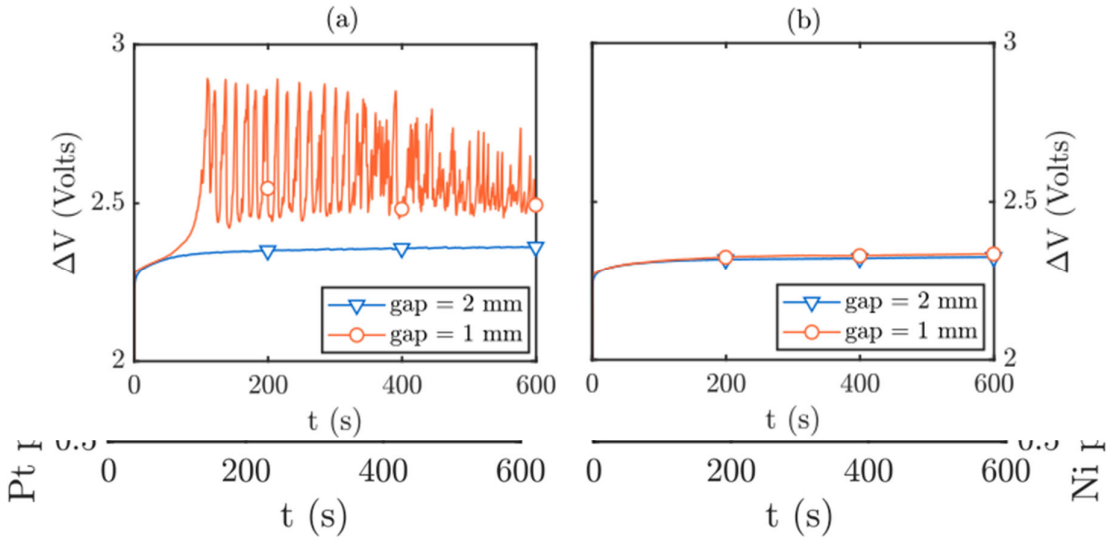

Figure 5: Chronopotentiometry of the Zn/O_2 battery at 20 mA/cm^2 for several gaps between the electrodes **(a)** Static electrolyte **(b)** Flowing electrolyte (Q=1.5 mL. s^{-1}.

therefore 4 times smaller in the case of the 2 mm gap. For a given flow rate, this should theoretically lead to an improved bubble departure at small gaps since the overall external force is higher. However, results in **Figure 5b** show nearly the same potentials for the 1 mm and 2 mm gaps. This last point highlights that the imposed flow rate induces a sufficient shear stress to evacuate most of the produced bubbles. The slight difference of 10 mV measured between the two signals could potentially come from higher shear stress and/or gap dependent electrolyte conductivity. Indeed, electrolyte conductivity is given by $R_e = \rho_e \frac{L}{A}$ where L is the gap between electrodes, A the area of the electrodes, and ρ_e the specific conductivity of the electrolyte. For highly concentrated electrolyte used in the present study ($8M\ KOH, \rho_e \sim 0.02\ \Omega\ m$) this relation gives $R_e \sim 1\ \Omega\ for\ 2$ mm gap and $R_e \sim 0.5\ \Omega$ for 1 mm gap. At 20 mA. cm^{-2}, the difference in electric potential between the two studied gaps should be around 30 mV. This analysis shows that the slight difference measured in **Figure 5b** could also be explained by conductivity variations between the 2 situations. Overall, this 10 mV difference is not significant compared to the other results of the present study, and flowing electrolyte is efficient for bubble evacuation for both gaps.

On the other hand, static electrolyte conditions in **Figure 5a** should not be submitted to the same rheological description. Indeed, without electrolyte flow, the shear stress should only be governed by the slight natural convection induced by bubble departure. In this situation the rheological parameters are only dependent on cell geometry. Reducing the gap should increase the overall hydraulic resistance as $R_h \propto {}^{1}/_{L^3}$. This relation underlines that bubble evacuation is improved with a 2 mm gap, as shown in **Figure 5a**. Indeed, with a 1 mm gap, the measured potential reaches high values and oscillates strongly. On the other hand, results using a 2 mm gap show that the evacuation by natural convection is efficient in these conditions.

This last analysis point out that a 2 mm gap should be preferential in static and flowing electrolyte. In flowing conditions, there is no electric difference between the 2 gaps, but the pressure drop is following $R_h \propto {}^{1}/_{L^3}$. Thus, the consumed power for the electrolyte flow also depends on ${}^{1}/_{L^3}$, it seems wise to increase the gap to reduce energy consumption. For the case of static electrolyte, increasing the gap from 1 to 2 mm reduce overpotential and electric stability, leading to an improved energy consumption as well.

Beyond the previous analysis, note that the limiting current for the experiments presented in **Figure 5a** should be given by $J_{lim} = 4D_{Zn(OH)_4^{2-}} F C_{Zn(OH)_4^{2-}} / L_{gap}$ which corresponds respectively to 10 and 5 mA. cm^{-2} for 1 and 2 mm gaps ($D_{Zn(OH)_4^{2-}} = 6\ 10^{-10}$ m^2/s) [13]. The applied current is thus higher than the calculated limiting one for both situations (gap 1 & 2 mm). The global overpotential should thus be higher for the 2 mm gap since the limiting current is 2 times lower than the 1 mm gap situation. However, we observe the opposite result in **Figure 5a**. Previous studies showed that this limiting current calculation underestimates the effective limiting current because of local convective vortex at electrodes surface [15]. The result in **Figure 5a** confirms this previous work since the overpotential using a 2 mm gap is lower than with 1 mm gap. The differences between the 2 gaps under static electrolyte is explained by the previous analysis: because of the modification of cell permeability, natural convection is stronger for large gaps and thus leads to higher shear stress at the electrode surface.

On the other hand, limiting current under flowing electrolyte (**Figure 5b**) differs: the relation $J_{lim} = 4D_{Zn(OH)_4^{2-}} F C_{Zn(OH)_4^{2-}} / L_{gap}$ cannot be applied since the convective flow of electrolyte allows to bring ions to the surface and increases drastically the limiting current [16]. (>100 mA. cm^{-2} in our conditions). In this situation, the applied current should be lower than the limiting one.

Discussion

Let us now comment all the experimental data seen in this study. The overall analysis of the results presented in this study allows to quantify and understand the different way to improve convection dynamics in multi-phasic electrochemical systems.

The approach used allows us to link electric performances (especially stability) with free surface variations for several geometries of electrochemical flow-cells and electrodes. As previously reported, electrolyte flow drastically enhances the performance of such systems. Moreover, it prevents from oscillating behavior and improves electrode stability. Despite this previously reported result, our experiments show that geometry of the flow cell is a crucial point to fully take advantage of flowing devices. This point is highlighted by **Figure 2**, where free surface and overpotential become highly different according to the used geometry. The importance of flow-cell geometry becomes higher at large current density, showing that well designed systems are necessary in order to perform efficient fast charges. Previous energy consumption analysis on this type of flowing designs showed that the energy consumption of the flow is neglectable compared to the energy gain induced by overpotential decrease [2]. Here, we showed in **Figure 4** that this energy gain can become much higher than previously reported results. Indeed, it can reach 70% of the overall electric consumption when processes are submitted to fast charge conditions.

From the eyes of industrial development and despite this energy gain under operating conditions, one could consider the cost of hydraulic equipment, of maintenance and the safety risks which can be added. In this regard, **Figure 3 and 4a** showed that microfluidic inspired design limits the unstable electrical evolution without electrolyte flow, even at fast

charges. However, the overpotential still reaches high values and its unstable behavior cannot be completely prevented, particularly at high currents.

Comparing natural and forced convection shows that electrolyte flow is much higher performant than any natural evacuation presented here. In this study, fast charge conditions cannot be reasonably achieved without flowing conditions (**Figure 4**). On the other hand, these results have shown the importance of geometry on convection for diphasic systems, and open the way to new and more efficient designs for natural evacuation of gas phases. In addition , numerical simulations [7] suggest an important role of electrode design, as confirmed by **Figure 4**. Modified electrode surface by the addition of heterogeneous properties of nucleation sites (wettability, passivation, rugosity…) combined to improved cell geometry could lead to efficient natural evacuation of gas phases.

We also show in this study that the distance between the electrodes is an important parameter (**Figure 5**). For static electrolyte, we showed that increasing the gap leads to better gas evacuation since it decreases hydraulic resistance of the cell, and thus allows faster natural convection. When the flow rate is imposed, the shear stress is higher in small gaps which should theoretically lead to better gas evacuation. However, in our conditions we observe no significant difference between 1 mm and 2 mm gap, meaning that the flowing conditions are sufficient here for the evacuation of most of the gas phase.

We showed that the flow and the geometry of the cell had a strong impact on the overpotentials. It is at this point important to recall another important parameter: the bubble size distribution. Simulations previously performed by our team [7] points out another way to improve natural convection towards electrode design and manufacturing. Indeed, even if we promote the use of an electrolyte flow, it is clear that improving the natural evacuation of bubbles from this way should equally increases the performance of such a cell with flow. The results suggest that heterogeneities on electrode surface can improve electric stability. Indeed, heterogeneities may induce bubbles with various size. A large size distribution will cause a large repartition of departure frequencies of bubbles at the electrodes and thus a smoother electrical signal. **Figure 6** represents some results of these simulations (reproduced with permission of the authors). **Figure 6a** shows the effect of external convection which induces a detachment radius decrease. The results are in agreement with experimental measures in **Figure 2-4**. On the other hand, **Figure 6b** shows the effect of surface heterogeneities on electrical oscillations. Wider repartition of nucleation sites properties induces wider repartition of frequency departure and enhances the stability of the electrode. Let us emphasize that numerical simulations taking into account the flow of the bubbles in the channel are required to give a comprehensive version of the process.

Conclusion

The analysis of diphasic electrochemical flow-processes presented in our work shows several ways to improve the gas phase evacuation involved in these systems. Linking

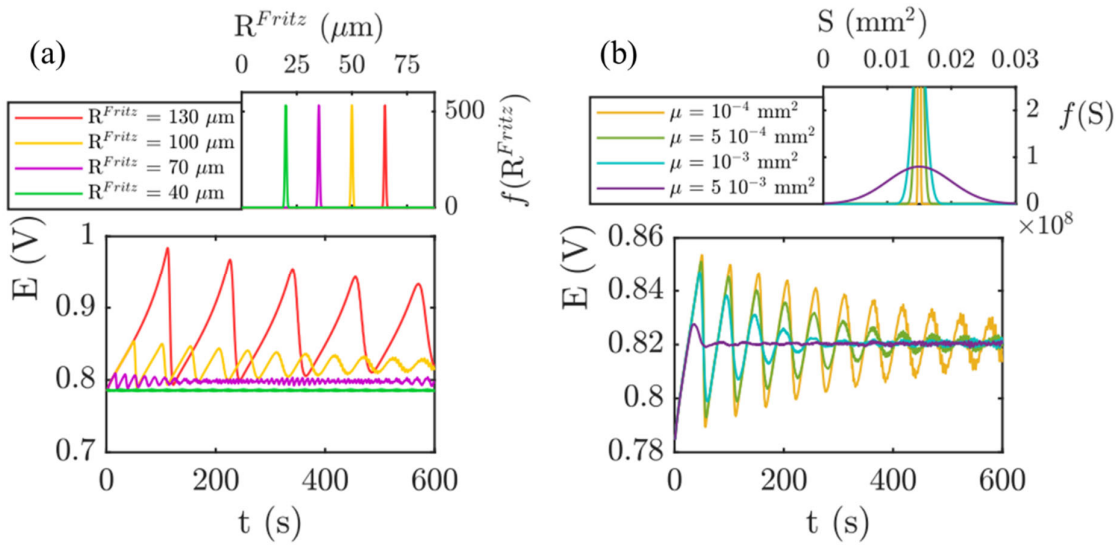

Figure 6: Numerical simulation from [7]. **(a)** Computed electrode electric potential under forced convection and **(b)** computed electrode potential for surface heterogeneities. It is assumed from the experiments that the Friz radius decreases as a function of the stress on the electrode.

electrode free surface to electrochemical kinetics allows us to estimate the covered area and highlights its harmful effect on performances. Theory predicts that these undesirable effects are especially high when the free surface oscillates towards 0. Experiments confirm these considerations and show that this behavior appears mostly at high currents which limits fast charge possibilities. As expected, electrolyte flow drastically reduces surface coverage and increases electric performances. Comparing cell geometries shows that flow-design is a key parameter for efficient forced convection. V-shaped millifluidic cells show good performances compared to previous results [2] and allow to perform fast-charge conditions without significant surface-overpotential. Regarding natural convection, this geometry has the benefits to limit the instabilities usually observed at high currents, suggesting favorable bubble detachment kinetics. Comparing natural and forced convection shows that electrolyte flow is clearly the more efficient way to improve performances and is the only way to perform efficient fast-charges in our systems.

Our last results under fast-charge conditions confirm that the role of the electrode design is an important parameter to consider. Thus, our experimental work combined to simulation results open the way to optimized systems, with improved flow geometry and electrode surface. Such systems could eventually lead to even faster charges without significant surface-overpotential and instabilities

Beside this consideration, numerical simulations show that the surface design of electrodes can improve the bubble detachment kinetics and limit instabilities. One way to do this is to create artificial sites of preferential nucleation on the electrode that set different Fritz radii. This can be performed by creating hydrophobic spots on electrodes [17]. This can be done by varying the wettability of the electrode (by oxidation) or by using cavities or particles to modify the geometry of the surface. Note that the creation of artificial nucleation sites is also an approach that allows in the context of porous electrodes to ensure that bubbles do not form in the pores. This limits the mechanical degradation of the porous electrode and facilitates their removal [18]. This work opens the door to the design of new performant electrodes. Last but not the least, in the perspective it is important to take into account that in some situations, the existence of triple line liquid-solid-gas may favor the catalysis of the reactions [17]. Numerical simulations of bubble flows in confined systems are also needed to understand how to promote bubble flow and eliminate them [20-22].

Conflicts of Interest

The authors declare no conflicts of interest.

Funding Statement

MF acknowledges funding from ED 394 PSL University.

Acknowledgments

The authors acknowledge the IPGG platform (UAR CNRS 3750) and IPGG Labex for technological support.

Copyright and Permissions

Figure 3 is reproduced from [7] with the permission of the authors.

References

1. Vogt H. Gas-evolving electrodes. Comprehensive Treatise of Electrochemistry: Electrodics: Transport. 1983:445-89.

2. Abdelghani-Idrissi S, Dubouis N, Grimaud A, Stevens P, Toussaint G, Colin A. Effect of electrolyte flow on a gas evolution electrode. Scientific Reports. 2021 Feb 25;11(1):4677.

3. Li J, Zhu Y, Chen W, Lu Z, Xu J, Pei A, et.al. Breathing-mimicking electrocatalysis for oxygen evolution and reduction. Joule. 2019 Feb 20;3(2):557-69.

4. Faber MS, Dziedzic R, Lukowski MA, Kaiser NS, Ding Q, Jin S. High-performance electrocatalysis using metallic cobalt pyrite (CoS2) micro-and nanostructures. Journal of the American Chemical Society. 2014 Jul 16;136(28):10053-61.

5. Lu Z, Zhu W, Yu X, Zhang H, Li Y, Sun X, et.al. Ultrahigh hydrogen evolution performance of under-water "superaerophobic" MoS2 nanostructured electrodes. Advanced Materials. 2014 May;26(17):2683-7.

6. Wang X, Fei Y, Chen J, Pan Y, Yuan W, Zhang LY, et.al. Directionally In Situ Self-Assembled, High-Density, Macropore-Oriented, CoP-Impregnated, 3D Hierarchical Porous Carbon Sheet Nanostructure for Superior Electrocatalysis in the Hydrogen Evolution Reaction. Small. 2022 Jan;18(2):2103866.

7. Wang X, Le JB, Fei Y, Gao R, Jing M, Yuan W, et.al. Self-assembled ultrasmall mixed Co–W phosphide nanoparticles on pristine graphene with remarkable synergistic effects as highly efficient electrocatalysts for hydrogen evolution. Journal of Materials Chemistry A. 2022;10(14):7694-704.

8. Eigeldinger J, Vogt H. The bubble coverage of gas-evolving electrodes in a flowing electrolyte. Electrochimica Acta. 2000 Sep 1;45(27):4449-56.

9. Abdelghani-Idrissi S, Colin A. Numerical computation of electrical potential on a gas evolving electrode. Scientific Reports. 2023 Jan 31;13(1):1722.

10. Hine F, Murakami K. Bubble effects on the solution IR drop in a vertical electrolyzer under free and forced convection. Journal of the Electrochemical Society. 1980 Feb 1;127(2):292.

11. Wang K, Pei P, Ma Z, Chen H, Xu H, Chen D, et.al. Growth of oxygen bubbles during recharge process in zinc-air battery. Journal of Power Sources. 2015 Nov 20;296:40-5.

12. Hine F, Yasuda M, Nakamura R, Noda T. Hydrodynamic Studies

of Bubble Effects on the IR-Drops in a Vertical Rectangular Cell. Journal of The Electrochemical Society. 1975 Sep 1;122(9):1185.

13. Rocha F, Delmelle R, Georgiadis C, Proost J. Effect of pore size and electrolyte flow rate on the bubble removal efficiency of 3D pure Ni foam electrodes during alkaline water electrolysis. Journal of Environmental Chemical Engineering. 2022 Jun 1;10(3):107648.

14. Lehmann W. Construction einer neuen Tafel für den lapsus ellipticus etc (Fortsetz. von Nr. 1048). Astronomische Nachrichten. 1856 Sep;44:261.

15. Ma MC, Li G, Chen X, Archer LA, Wan J. Suppression of dendrite growth by cross-flow in microfluidics. Science Advances. 2021 Feb 19;7(8):eabf6941.

16. Ito Y, Wei X, Desai D, Steingart D, Banerjee S. An indicator of zinc morphology transition in flowing alkaline electrolyte. Journal of Power Sources. 2012 Aug 1;211:119-28.

17. Brussieux C, Viers P, Roustan H, Rakib M. Controlled electrochemical gas bubble release from electrodes entirely and partially covered with hydrophobic materials. Electrochimica Acta. 2011 Aug 1;56(20):7194-201.

18. Kadyk T, Bruce D, Eikerling M. How to enhance gas removal from porous electrodes?. Scientific Reports. 2016 Dec 23;6(1):1-4.

19. Ciampi S, Iyer KS. Bubbles pinned on electrodes: Friends or foes of aqueous electrochemistry?. Current Opinion in Electrochemistry. 2022 Mar 29:100992.

20. Anna SL. Droplets and bubbles in microfluidic devices. Annual Review of Fluid Mechanics. 2016 Jan 3;48:285-309.

21. Hourtane V, Bodiguel H, Colin A. Dense bubble traffic in microfluidic loops: Selection rules and clogging. Physical Review E. 2016 Mar 15;93(3):032607.

22. Huang C, Wippold JA, Stratis-Cullum D, Han A. Eliminating air bubble in microfluidic systems utilizing integrated in-line sloped microstructures. Biomedical Microdevices. 2020 Dec;22:1-9.